11th International Symposium on Turbulence and Shear Flow Phenomena (TSFP11)
Southampton, UK, July 30 to August 2, 2019

RESPONSE OF A FLEXIBLE WALL TO TURBULENT CHANNEL FLOW

Sreevatsa Anantharamu
Aerospace Engineering and Mechanics
University of Minnesota
110 Union St SE, Minneapolis, MN 55414
anant035@umn.edu

Krishnan Mahesh
Aerospace Engineering and Mechanics
University of Minnesota
110 Union St SE, Minneapolis, MN 55414
kmahesh@umn.edu

ABSTRACT

We discuss one-way coupled results of an elastic plate excited by wall-pressure fluctuations generated by Direct Numerical Simulation (DNS) of turbulent channel flow at Re_τ of 180 and 400, where $Re_\tau := \frac{u_\tau \delta}{\nu}$, u_τ is the friction velocity, δ is the half channel height and ν is the kinematic viscosity of the fluid. We present a novel framework to compute the magnitude and phase of the wall-normal distribution of the dominant flow sources to the modal force power spectral density (PSD) of the plate. This developed framework is also used to obtain the characteristics of the dominant sources in the channel that contribute to the wall-pressure fluctuation PSD. The wall-pressure fluctuations show a collapse in the spanwise similarity functions for both Re_τ at high frequencies. The computed averaged displacement power spectral density of the clamped plate varies roughly as ω^{-9} around $\omega\delta/u_\tau = 100$ for both Re_τ. The domain within the boundary layer that contributes to the modal force PSD of the plate is maximum near the hydrodynamic coincidence frequency of the plate at $Re_\tau = 180$. The computed dominant source distribution for wall-pressure fluctuations show that the region around $y^+ \approx 6$ contributes to the PSD for both low and high frequency whereas the contribution of the outer region diminishes with increasing frequency. At low frequencies for $Re_\tau = 180$, there is a pair of dominant regions around $y^+ \approx 40$ which are opposite in phase with each other that contribute to wall-pressure fluctuation.

INTRODUCTION

Structural vibrations due to turbulent boundary layer (TBL) wall-pressure fluctuations contribute to radiated far-field sound. For sufficiently small response of the structure, the coupling between the boundary layer and structural response can be assumed to be one-way coupled. For a flat plate excited by a TBL, the wavenumber frequency spectrum of wall-pressure fluctuation determines the structural response. Several experiments (Willmarth & Wooldridge (1962), Corcos (1964), Blake (1970), Farabee & Casarella (1991)) and Direct Numerical Simulations (DNS) (Kim (1989), Choi & Moin (1990), Hu *et al.* (2006), Sillero *et al.* (2013)) have been carried out to characterize the wall-pressure fluctuations in an incompressible TBL. Readers are referred to the comprehensive reviews by Willmarth (1975), Bull (1996) and Blake (2017) for more details on TBL wall-pressure fluctuations. The one-way coupled response of elastic plates subjected to homogenous TBL wall-pressure fluctuations have been previously studied using Frequency domain Finite Element Method (FEM) calculations (Hambric *et al.*, 2004). The one-way coupling between the wall-pressure fluctuations and an elastic plate have been analyzed previously using modal sensitivity functions (Blake (2017); Hwang & Maidanik (1990)).

In this paper, we perform time-domain FEM simulations to obtain the one-way coupled plate response due to excitation from TBL wall-pressure flucutations at $Re_\tau = 180$ and 400. The wall-pressure flucutations are generated from DNS of turbulent channel flow. The bottom wall of the channel is assumed to be flexible. We present a novel framework to analyze the coupling between different portions in TBL and the plate utilizing the 3D DNS data, pressure fluctuation Poisson equation source terms, and Spectral Proper Orthogonal Decomposition (SPOD) (Towne *et al.*, 2018). The analysis yields the magnitude and phase of the wall-normal distribution of the dominant sources (through SPOD modes) within the channel to the modal force spectral density of the plate and also to the wall-pressure fluctuation PSD. These SPOD modes help to understand the coupling between coherent structures in TBL and the structural response.

The paper is organized as follows. First, we discuss the fluid and solid simulation methodologies. Then, we present the novel one-way coupled analysis framework. The obtained wall-pressure fluctuations, plate response and the one-way coupling between them is then analyzed.

METHODOLOGY

Simulation details

DNS of turbulent channel flow is performed by solving the incompressible Navier-Stokes equations using the finite volume method of Mahesh *et al.* (2004) in a convecting frame of reference moving with the bulk velocity of the fluid in the channel. The semi-discrete (space only discretization) form of the method is discretely kinetic energy conserving. The moving reference frame was seen to yield better prediction of the high wavenumber region of the velocity fluctuation spectra (Bernardini *et al.*, 2014). Time integration is performed using the Crank-Nicholson scheme. The governing equations are non-dimensionalized based on friction velocity (u_τ) and half channel height (δ). The computational domain is chosen to be a box $6\pi\delta \times 2\delta \times 2\pi\delta$ for both $Re_\tau = 180$ and 400, where $6\pi\delta, 2\pi\delta$ and 2δ are

Table 1: Grid size for the fluid DNS and solid simulations. Superscript f denotes fluid and s denotes solid. Here, we choose x, y and z to be streamwise, wall-normal and spanwise direction respectively.

Re_τ	$N_x^f \times N_y^f \times N_z^f$	$N_x^s \times N_y^s \times N_z^s$
180	$720 \times 176 \times 330$	$144 \times 1 \times 66$
400	$1388 \times 288 \times 660$	$347 \times 1 \times 165$

the lengths in the streamwise, spanwise and wall-normal directions. The computational mesh (table 1) is uniform in streamwise and spanwise direction and we use a hyperbolic tangent spacing in the wall-normal direction with a stretching factor of 2.07 for both Re_τ. The mesh spacing is fine enough to resolve the structures in the channel. A time step of $5 \times 10^{-4} \nu / u_\tau^2$ is used for both Re_τ. The mean and root mean square (RMS) statistics of velocities are validated with the DNS results of Moser *et al.* (1999) (not shown). The DNS simulation is run for a total time of 10 units after the initial transients settle down. The pressure fluctuation on the bottom wall is stored for every time step and is used to excite the linear elastic plate. The source term of the pressure fluctuation Poisson equation is also stored every time step for the one-way coupling analysis described in the subsequent sections.

The dynamic linear elasticity equations are solved using continuous Galerkin Finite Element Method in space and Newmark time integration scheme (Hughes, 2012). We use hexahedral elements with polynomials of degree 2 to represent the approximate solution within each element. The description and validation of the solver for static, dynamic and eigenvalue problems is discussed in Anantharamu & Mahesh (2018). The plate at the bottom wall is clamped on all sides. The pressure fluctuations from the fluid solver are imposed onto the plate as wall-normal traction. The fluid and solid grids are chosen such that the fluid surface mesh is a refinement of the solid surface mesh at the interface. For such a configuration, we use an optimal methodology described in Anantharamu & Mahesh (2018) to transfer the piecewise constant representation of the pressure in the fluid domain onto the solid domain. Also, we use an in-house implementation of the preconditioner described in Klöppel *et al.* (2011) to address the high condition number arising from the aspect ratio of the elements due to the thin plate geometry. The solution time of the linear algebra problem is reduced by $30-40\%$ due to the preconditioner. The solid mesh sizes used for the $Re_\tau = 180$ and 400 simulations is mentioned in table 1. We choose a half channel height of $2.5cm$. The plate thickness (h), Young's modulus (E), Poisson ratio (ν_s) and density (ρ_s) of the plate is chosen to be $0.1cm$, $10MPa$, 0.4 and $1200kgm^{-3}$ respectively. A mass proportional damping is assumed that yields a structural loss factor of 0.05 at the first natural frequency. The kinematic viscosity of the fluid is assumed to be $1.1 \times 10^{-6} m^2 s^{-1}$.

One-way coupling analysis framework

We analyze the one-way coupling between the channel and the plate as follows. We compute complex wall-normal modes and their corresponding eigenvalues using SPOD of wall-normal cross-spectral density of the contribution of the sources within the channel to the modal force PSD. The same framework can be used to understand the wall-normal correlated contribution to the wall-pressure fluctuation PSD.

The modal force PSD $\phi_{pp}^{m,n}(\omega)$ for the $(m,n)^{th}$ mode of the plate is defined as (Blake, 2017)

$$\phi_{pp}^{m,n}(\omega) = \int_\Gamma \int_\Gamma \Phi_{pp}(\mathbf{x}_1, \mathbf{x}_2, \omega) \psi_{m,n}(\mathbf{x}_1) \psi_{m,n}(\mathbf{x}_2) \mathrm{d}\mathbf{x}_1 \mathrm{d}\mathbf{x}_2, \tag{1}$$

where Γ is the plate surface, m and n are the mode indices in streamwise and spanwise directions respectively, $\Phi_{pp}(\mathbf{x}_1, \mathbf{x}_2, \omega)$ is the cross-spectral density of the wall-pressure fluctuations, $\psi_{m,n}(\mathbf{x})$ is the $(m,n)^{th}$ mode shape of the plate. Assuming homogeneity in the streamwise and spanwise directions, we use Fourier transforms to rewrite $\phi_{pp}^{m,n}(\omega)$ as an integral over the spanwise and streamwise wavenumbers as

$$\begin{aligned} \phi_{pp}^{m,n}(\omega) &= \int_{-\infty}^{\infty} \int_{-\infty}^{\infty} \Phi_{pp}(\mathrm{k}_1, \mathrm{k}_3, \omega) |S_{m,n}(\mathrm{k}_1, \mathrm{k}_3)|^2 \mathrm{d}\mathrm{k}_1 \mathrm{d}\mathrm{k}_3, \\ S_{m,n}(\mathrm{k}_1, \mathrm{k}_3) &:= \int_\Gamma \psi_{m,n}(\mathrm{x}_1, \mathrm{x}_3) e^{-i(\mathrm{k}_1 \mathrm{x}_1 + \mathrm{k}_3 \mathrm{x}_3)} \mathrm{d}\mathrm{x}_1 \mathrm{d}\mathrm{x}_3 \end{aligned} \tag{2}$$

where $\Phi_{pp}(\mathrm{k}_1, \mathrm{k}_3, \omega)$ is the wall-pressure fluctuation wavenumber frequency spectrum. In equation 2, $|S_{m,n}(\mathrm{k}_1, \mathrm{k}_3)|^2$ is called the modal sensitivity function (Blake, 2017). $\Phi_{pp}(\mathrm{k}_1, \mathrm{k}_3, \omega)$ can be related to the wall-normal cross-spectral density of source terms of the pressure fluctuation Poisson equation $\phi_{ff}(\mathrm{k}_1, \mathrm{k}_3, \mathrm{r}, \mathrm{s}, \omega)$ using the Green's function of the Poisson problem for the channel flow domain. The modal PSD then becomes

$$\begin{aligned} \phi_{pp}^{m,n}(\omega) &= \int_{-1}^{+1} \int_{-1}^{+1} \Gamma_{m,n}(\mathrm{r}, \mathrm{s}, \omega) \mathrm{d}\mathrm{r}\mathrm{d}\mathrm{s}, \\ \Gamma_{m,n}(\mathrm{r}, \mathrm{s}, \omega) &:= \int_{-\infty}^{\infty} \int_{-\infty}^{\infty} G(0, \mathrm{r}, \mathrm{k}_1, \mathrm{k}_3) G(0, \mathrm{s}, \mathrm{k}_1, \mathrm{k}_3) \\ &\qquad \phi_{ff}(\mathrm{k}_1, \mathrm{k}_3, \mathrm{r}, \mathrm{s}, \omega) |S_{m,n}(\mathrm{k}_1, \mathrm{k}_3)|^2 \mathrm{d}\mathrm{k}_1 \mathrm{d}\mathrm{k}_3, \end{aligned} \tag{3}$$

where $\Gamma_{m,n}(\mathrm{r}, \mathrm{s}, \omega)$ is the contribution of sources correlated at wall-normal locations r and s in the boundary layer which is computed from the DNS data, $G(0, \mathrm{r}, \mathrm{k}_1, \mathrm{k}_3)$ is the Green's function with one point fixed at wall. In order to obtain the distribution of the dominant contribution, we perform spectral POD of $\Gamma_{m,n}(\mathrm{r}, \mathrm{s}, \omega)$ as

$$\Gamma_{m,n}(\mathrm{r}, \mathrm{s}, \omega) = \sum_{i=1}^{\infty} \lambda_i(\omega) \varphi_i(\mathrm{r}, \omega) \varphi_i^*(\mathrm{s}, \omega), \tag{4}$$

where $(\lambda_i(\omega), \varphi_i(\mathrm{r}, \omega))$ are the spectral POD eigenvalue and eigenvector pairs. The modal PSD can then be written as

$$\begin{aligned} \phi_{pp}^{m,n}(\omega) &= \sum_{i=1}^{\infty} \gamma_i(\omega), \\ \gamma_i(\omega) &:= \lambda_i(\omega) \left| \int_{-1}^{+1} \varphi_i(\mathrm{r}, \omega) \mathrm{d}\mathrm{r} \right|^2 \end{aligned} \tag{5}$$

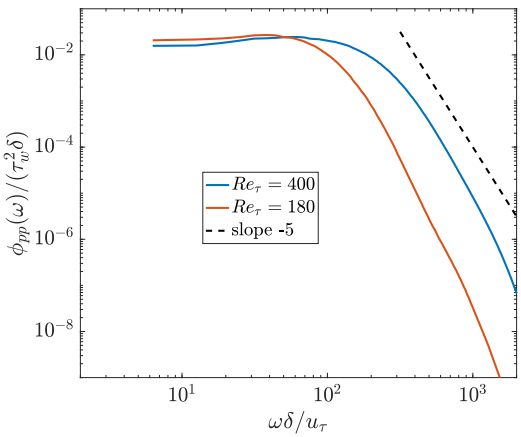

Figure 1: Comparison of wall-pressure fluctuation power spectral density.

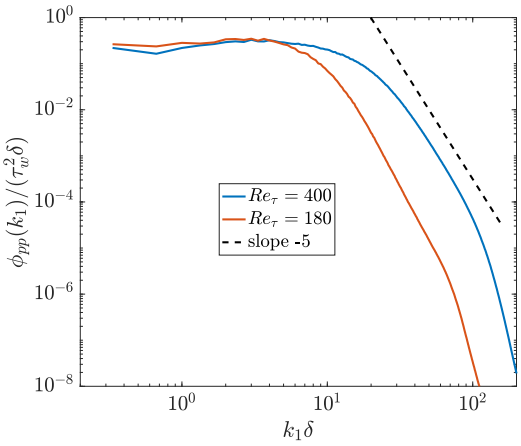

Figure 2: Comparison of wall-pressure fluctuation streamwise wavenumber spectra.

We can also write the modal PSD as

$$\phi_{pp}^{m,n}(\omega) = \int_{-1}^{+1} \Psi_{m,n}(\mathrm{r},\omega)\mathrm{dr},$$
$$\Psi_{m,n}(\mathrm{r},\omega) := Re\left(\int_{-1}^{+1} \Gamma_{m,n}(\mathrm{r},\mathrm{s},\omega)\mathrm{ds}\right). \quad (6)$$

$\gamma_i(\omega)$ yields the contribution of each SPOD mode to the modal PSD. The dominant SPOD mode at a given frequency will have larger value of $\gamma_i(\omega)$. We can also view the set of numbers $\{\gamma_i(\omega)\}_{i=1}^{\infty}$ as a modal wall-normal PSD of the plate. The corresponding SPOD mode yields the magnitude and phase of the dominant sources in the wall-normal direction. The function $\Psi_{m,n}(\mathrm{r},\omega)$ gives the wall-normal distribution of the integrated contribution of all sources to the modal PSD of the plate at a given frequency.

Repeating the above analysis by setting $S_{m,n}(k_1,k_3,\omega) = 1$ yields information on sources that contribute to the wall-pressure fluctuation PSD. So, we define $S_{0,0}(k_1,k_3,\omega)$ to be 1 since the mode indices m and n of the plate begin from 1. The analysis required $13TB$ of data for $Re_\tau = 180$ and a parallel implementation was therefore developed. The one-way coupling analysis is currently being extended to relate the far-field radiated sound from wall vibration to sources within the channel.

RESULTS AND DISCUSSION

Wall-pressure fluctuation

We first show statistics of wall-pressure fluctuations at $Re_\tau = 180$ and 400. Figures 1 and 2 show the PSD and streamwise wavenumber spectra respectively. The low frequency region of the power spectral density appear to collapse well for both Re_τ whereas the high-frequency region differs due to the non-dimensionalization using outer units. The high frequency region is seen to decay with slope -5, especially for the higher Re_τ case. The collapse in the high frequency region would be better if the PSD is plotted in viscous units. The streamwise wavenumber spectral density show the same trend as that of the PSD. The -5 decay in the high wavenumber region is clearly evident from figure 2.

Most turbulent boundary layer wall-pressure fluctuation models for wavenumber frequency spectrum are given in terms of streamwise and spanwise similarity functions (Blake, 2017) $F_1(k_1U_c/\omega)$ and $F_3(k_3U_c/\omega)$ defined as

$$F_1(k_1U_c/\omega) := \Phi_{pp}(k_1,\omega)\omega/(\phi_{pp}(\omega)U_c(\omega)),$$
$$F_3(k_3U_c/\omega) := \Phi_{pp}(k_3,\omega)\omega/(\phi_{pp}(\omega)U_c(\omega)), \quad (7)$$

where the convection velocity $U_c(\omega)$ is defined as $U_c(\omega) := \omega/k_{max}$, k_{max} is the wavenumber with maximum value of streamwise wavenumber frequency spectrum for fixed ω. For $Re_\tau = 180$ and 400, $U_c(\omega)/U_o$ is around 0.8 and 0.7 (for high frequency range) respectively (not shown). In figure 3a and 3b, we plot the streamwise and spanwise similarity function for both Re_τ for different frequencies. The spanwise similarity function collapses for both Re_τ at high frequencies whereas the streamwise similarity function does not show collapse except in the immediate vicinity of $k_1U_c(\omega)/\omega = 1$. Also, the spurious high magnitude of the streamwise similarity function for low k_1U_c/ω attributed to artifical acoustics as discussed in Choi & Moin (1990) is not seen in the present calculations. We believe that our large domain size eliminated any feedback effect from periodic boundary conditions which was deduced to be the reason for the spurious high values in Choi & Moin (1990).

Plate response

We compare the response of the FEM clamped plate to Poisson-Kirchoff plate theory for simply supported BC. The Poisson- Kirchoff plate theory simulation used the modified Corcos form (Hwang & Maidanik, 1990) of the wavenumber frequency spectrum with DNS wall-pressure fluctuation PSD. Figure 4 shows the plate averaged displacement spectra $\phi_{dd}^a(\omega)$ for $Re_\tau = 180$ and 400. The plate average response increases with Re_τ as the pressure fluctuations get stronger with increasing Re_τ. We see that in the frequency range around 100, the plate averaged response varies roughly as ω^{-9}. Table 2 shows the comparison of the non-dimensional RMS normal displacement and velocity for the different cases. The RMS normal displacement $< d_n^2 >^{1/2}/\delta_\nu$ varies between 0.07-2. Also, the RMS normal velocity $< v_n^2 >^{1/2}/u_\tau$ of the plate is around 0.003-0.065. Such small values of the plate response in viscous units justify the one-way coupled analysis.

Note that here the physical (dimensional) values of

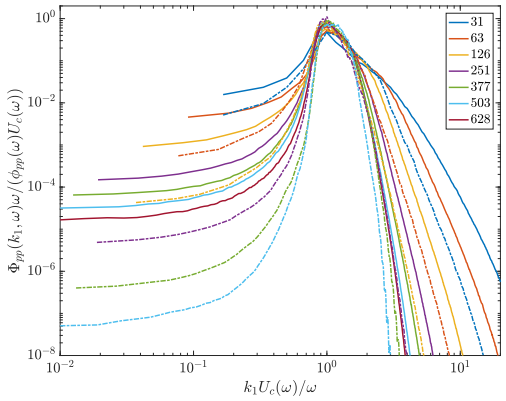

(a) Streamwise similarity function.

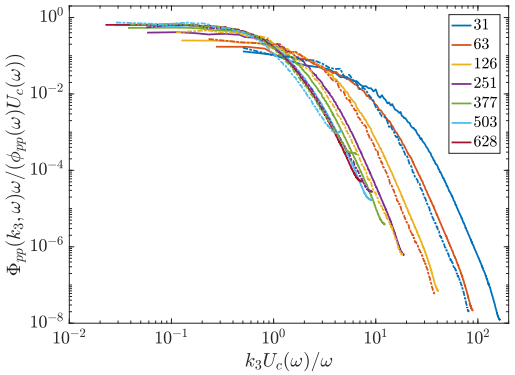

(b) Spanwise similarity function

Figure 3: Streamwise and spanwise similarity function for $Re_\tau = 180$ and 400 for several $\frac{\omega\delta}{u_\tau}$. *Solid* lines denote $Re_\tau = 180$ and *dashed-dotted* lines denote $Re_\tau = 400$. $\frac{\omega\delta}{u_\tau}$ is color coded as shown in legend for both cases.

Young's modulus is kept constant for both Re_τ. In non-dimensional units, $E/\left(\rho_f u_\tau^2\right)$ decreases with Re_τ as u_τ increases. So, the non-dimensional natural frequencies of the plate and the associated peaks in the spectra shift to the lower end of the spectrum as the plate becomes softer in non-dimensional units with increasing Re_τ. For each Re_τ, the simply supported plate vibrates more than clamped plate as it is less stiff.

Table 2: Average Root Mean Square (RMS) normal displacement $< d_n^2 >^{1/2} /\delta_\nu$ and velocity $< v_n^2 >^{1/2} /u_\tau$ of the plate in viscous units.

Case	$< d_n^2 >^{1/2} /\delta_\nu$	$< v_n^2 >^{1/2} /u_\tau$
$Re_\tau = 180, FEMC$	0.0719	0.0028
$Re_\tau = 180, PKSS$	0.1136	0.0054
$Re_\tau = 400, FEMC$	0.4319	0.0139
$Re_\tau = 400, PKSS$	2.1544	0.0645

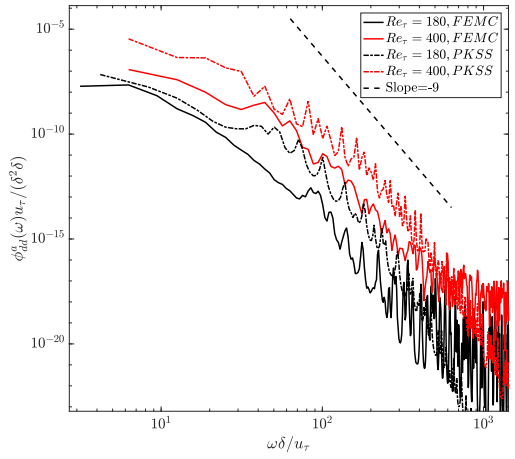

Figure 4: Comparison of plate averaged displacement power spectral density for $Re_\tau = 180$ and 400. *FEMC* denotes case using Finite Element Method with clamped plate BC and *PKSS* denotes case using Poisson-Kirchoff plate theory using simply-supported BC.

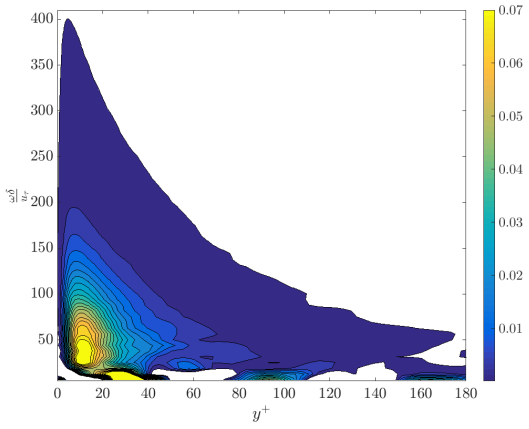

Figure 5: Contour plot of wall-normal distribution of net contribution of sources ($\Psi_{0,0}(y,\omega)$) to wall-pressure fluctuation PSD for different frequencies at $Re_\tau = 180$. Contour lines are 20 linearly spaced values between 0.0002 and 0.07.

One-way coupling analysis

We first present the distribution of the sources that contribute to wall-pressure fluctuation PSD based on the framework discussed in the previous section. Then, we present the analysis for the modal PSD of a simply supported mode shape with mode indices $m = 29$ and $n = 1$.

Figure 5 shows the wall-normal distribution of $\Psi_{0,0}(y,\omega)$ to wall-pressure fluctuation PSD for different frequencies at $Re_\tau = 180$. The dominant contribution in the frequency range ($25 < \omega\delta/u_\tau < 200$) is seen to be from the buffer layer ($5 < y^+ < 30$) and the exact location of the peak contribution moves towards the edge of the buffer and viscous layer as frequency increases. The outer region of the boundary layer is seen to make some contribution only to the low frequency of range of the spectrum. Sources at $y^+ = 50$ are seen to contribute the most at low frequency

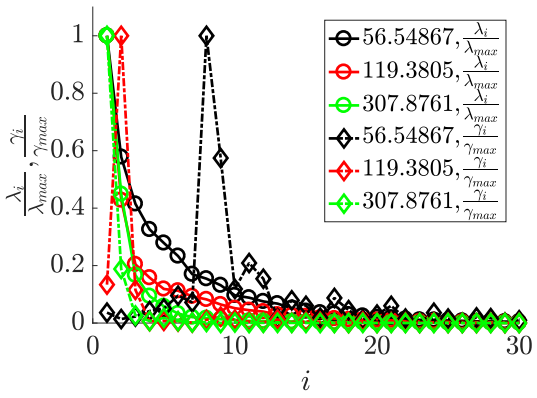

Figure 6: Normalized SPOD eigenvalues (λ_i/λ_{max}) and contribution to wall pressure fluctuation PSD (γ_i/γ_{max}) for different frequencies at $Re_\tau = 180$. Frequency $\frac{\omega\delta}{u_\tau}$ is color coded as shown in legend.

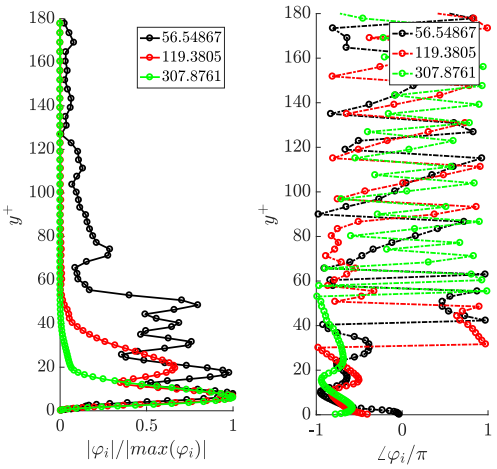

Figure 7: Magnitude and phase of the dominant SPOD mode shapes for 3 different frequencies at $Re_\tau = 180$ that contribute to wall-pressure fluctuation PSD with the largest value of $\gamma_i(\omega)$. Frequency $\frac{\omega\delta}{u_\tau}$ is color coded as shown in legend.

$\omega\delta/u_\tau \approx 44$.

The spectral POD eigenvalues λ_i and the wall-normal modal PSD γ_i of each SPOD mode is plotted in figure 6 normalized with the corresponding maximum values. As frequency increases, the number of spectral POD modes with eigenvalues larger than 10% of the peak value decreases i.e. fewer number of spectral POD modes are important. Also, for low frequencies, from the variation of λ_i/λ_{max}, we see that the dominant SPOD mode need not contribute most to the wall-pressure fluctuation PSD. This is because these dominant SPOD modes are oscillatory in nature (not shown here) leading to small values of $|\int_{-1}^{+1}\varphi_i(\mathrm{r},\omega)\mathrm{dr}|^2$ in equation 5.

Figure 7 shows the magnitude and phase of the dominant SPOD mode shapes that contribute to the wall-pressure fluctuation PSD chosen with the maximum value of $\gamma_i(\omega)$ for three different frequencies. We see from the variation of the magnitude of the mode shape that at all the three frequencies there is a peak around $y+ \approx 6$. The source of this

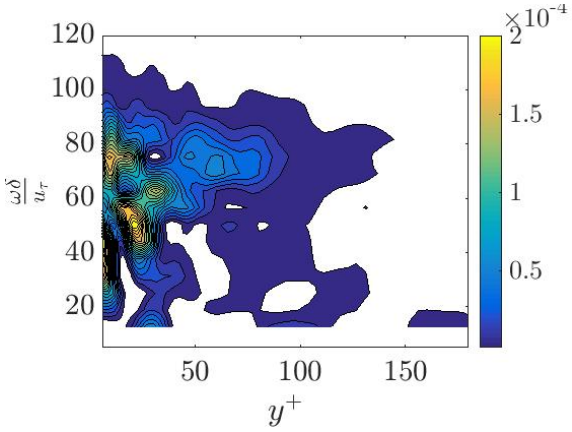

Figure 8: Contour plot of wall-normal distribution of net contribution of sources ($\Psi_{29,1}(y,\omega)$) to modal force PSD with $m = 29, n = 1$ for simply supported plate for different frequencies at $Re_\tau = 180$. Contour lines are 20 linearly spaced values between 1e-6 and 2e-4.

peak can possibly be attributed to the near wall shear layers based on its location alone. In the low frequency case, we see peaks at $y^+ \approx 50$ and $y^+ \approx 60$ which are out of phase by π radians. For the two low frequencies $\omega\delta/u_\tau \approx 57$ and 120, we see a secondary peak around $y^+ = 20$ whose contribution is in phase with the peak in the near wall region at $y^+ \approx 6$.

Next, we consider a simply supported mode with mode indices $m = 29$ and $n = 1$ with mode shape $\psi_{29,1}(\mathrm{x}_1,\mathrm{x}_3) = sin(\pi 29\mathrm{x}_1/\mathrm{L}_1)sin(\pi\mathrm{x}_3/\mathrm{L}_3)$. The wall-normal distribution of net contribution of sources ($\Psi_{29,1}(y,\omega)$) to modal force PSD for different frequencies at $Re_\tau = 180$ is shown in figure 8. It can seen be from the figure that around $\omega\delta/u_\tau \approx 75$, the range of y^+ that contributes to the function $\Psi_{29,1}(y,\omega)$ is maximum. This is due to hydrodynamic coincidence. At this frequency, the streamwise bending wavenumber of the plate for the considered mode $k_b = 29\pi/L_1$ is same as the convective wavenumber of the wall-pressure fluctuations $k_c = \omega/U_c$. So, the plate is receptive to forcing at this frequency than at other frequencies. The modal force PSD also has a maximum at this frequency (not shown).

Figure 9 shows the magnitude and phase of the dominant SPOD mode shapes that contribute to the modal force PSD for three different frequencies. The collapse in the normalized mode shape as seen for the dominant mode shapes that contribute to wall-pressure fluctuation PSD is not seen in figure 9. Even though the mode shapes for the two least frequency cases ($\omega\delta/u_\tau \approx 43, 50$) seem active above $y^+ = 50$, this portion does not significantly contribute to modal force PSD due to the linear variation of phase. The plotted SPOD mode at hydrodynamic coincidence frequency $\omega\delta/u_\tau \approx 75$ shows that the dominant sources within the TBL are spread over a maximum range of wall-normal locations which extend upto the outer layer. Currently, we are performing one-way coupling analysis at higher $Re_\tau = 400$.

CONCLUSION

We have discussed the response of plates subjected to wall-pressure fluctuations from DNS of turbulent channel

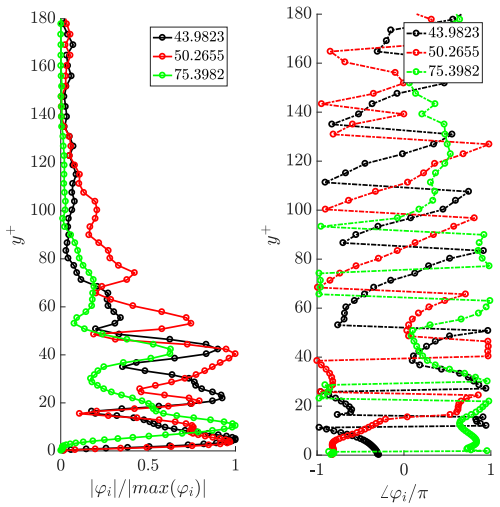

Figure 9: Magnitude and phase of the dominant SPOD mode shapes for 3 different frequencies at $Re_\tau = 180$ that contribute to modal force PSD $(m = 29, n = 1)$ with the largest value of $\gamma_i(\omega)$. Frequency $\frac{\omega\delta}{u_\tau}$ is color coded as shown in legend.

flow at $Re_\tau = 180$ and 400. We present a framework to analyze the one-way coupling between the TBL in channel and the plate. The response of the plate shows an approximate behavior of ω^{-9} in the frequency around $\omega\delta/u_\tau \approx 100$ for both Re_τ. The one-way coupling framework quantitatively shows that at hydrodynamic coincidence frequency the portion of the boundary layer that contributes to the modal force PSD for the chosen well excited mode of the plate is maximum. Analysis of wall-pressure fluctuation PSD using the same framework shows that the near-wall region $(y^+ \approx 6)$ contributes at all the frequencies considered whereas the contribution of the outer-layer diminishes with increasing frequency.

ACKNOWLEDGEMENT

This work is supported by the Office of Naval Research under grant N00014-17-1-2939 with Dr. Ki-Han Kim as technical monitor. The computations were made possible through computing resources provided by the US Army Engineer Research and Development Center (ERDC) in Vicksburg, Mississipi on the Cray XE6, Copper and Onyx of the High Performance Computing Modernization Program.

REFERENCES

Anantharamu, S & Mahesh, K. 2018 Time domain numerical simulation of elastic plate subjected to turbulent boundary layer wall–pressure fluctuations. In *32nd Symposium on Naval Hydrodynamics, Hamburg, Germany, Aug*.

Bernardini, Matteo, Pirozzoli, Sergio & Orlandi, Paolo 2014 Velocity statistics in turbulent channel flow up to $\mathrm{Re}_\tau = 4000$. *Journal of Fluid Mechanics* **742**, 171–191.

Blake, W. K. 1970 Turbulent boundary-layer wall-pressure fluctuations on smooth and rough walls. *Journal of Fluid Mechanics* **44** (4), 637–660.

Blake, W. K. 2017 *Mechanics of Flow-Induced Sound and Vibration, Volume 1 and 2.*. Academic Press.

Bull, M. K. 1996 Wall-pressure fluctuations beneath turbulent boundary layers: some reflections on forty years of research. *Journal of Sound and Vibration* **190** (3), 299–315.

Choi, H. & Moin, P. 1990 On the space-time characteristics of wall-pressure fluctuations. *Physics of Fluids A: Fluid Dynamics* **2** (8), 1450–1460.

Corcos, G. M. 1964 The structure of the turbulent pressure field in boundary-layer flows. *Journal of Fluid Mechanics* **18** (3), 353–378.

Farabee, T. M. & Casarella, M. J. 1991 Spectral features of wall pressure fluctuations beneath turbulent boundary layers. *Physics of Fluids A: Fluid Dynamics* **3** (10), 2410–2420.

Hambric, S. A., Hwang, Y. F. & Bonness, W. K. 2004 Vibrations of plates with clamped and free edges excited by low-speed turbulent boundary layer flow. *Journal of Fluids and Structures* **19** (1), 93–110.

Hu, Z., Morfey, C. L. & Sandham, N. D. 2006 Wall pressure and shear stress spectra from direct simulations of channel flow. *AIAA Journal* **44** (7), 1541–1549.

Hughes, T. J. R. 2012 *The finite element method: linear static and dynamic finite element analysis*. Courier Corporation.

Hwang, Y. F. & Maidanik, G. 1990 A wavenumber analysis of the coupling of a structural mode and flow turbulence. *Journal of Sound and Vibration* **142** (1), 135–152.

Kim, J. 1989 On the structure of pressure fluctuations in simulated turbulent channel flow. *Journal of Fluid Mechanics* **205**, 421–451.

Klöppel, Thomas, Gee, Michael W & Wall, Wolfgang A 2011 A scaled thickness conditioning for solid-and solid-shell discretizations of thin-walled structures. *Computer Methods in Applied Mechanics and Engineering* **200** (9-12), 1301–1310.

Mahesh, K., Constantinescu, G. & Moin, P. 2004 A numerical method for large-eddy simulation in complex geometries. *Journal of Computational Physics* **197** (1), 215–240.

Moser, Robert D, Kim, John & Mansour, Nagi N 1999 Direct numerical simulation of turbulent channel flow up to Re_τ= 590. *Physics of fluids* **11** (4), 943–945.

Sillero, J. A., Jiménez, J. & Moser, R. D. 2013 One-point statistics for turbulent wall-bounded flows at Reynolds numbers up to δ+ 2000. *Physics of Fluids* **25** (10), 105102.

Towne, Aaron, Schmidt, Oliver T & Colonius, Tim 2018 Spectral proper orthogonal decomposition and its relationship to dynamic mode decomposition and resolvent analysis. *Journal of Fluid Mechanics* **847**, 821–867.

Willmarth, W. W. 1975 Pressure fluctuations beneath turbulent boundary layers. *Annual Review of Fluid Mechanics* **7** (1), 13–36.

Willmarth, W. W. & Wooldridge, C. E. 1962 Measurements of the fluctuating pressure at the wall beneath a thick turbulent boundary layer. *Journal of Fluid Mechanics* **14** (2), 187–210.